Published in final edited form as:
Biomaterials. 2021 January 01; 266: 120432. doi:10.1016/j.biomaterials.2020.120432.

Π-Conjugated Polymeric Micelles Potentiate Docetaxel Therapy in Advanced-Stage Gastrointestinal Cancer

Chenghua Liang[#1], **Xiangyang Bai**[#2], **Cuiling Qi**[#3], **Qingxue Sun**[2], **Xiaoyan Han**[4], **Tianyun Lan**[4], **Haibo Zhang**[4], **Xiaoming Zheng**[1], **Rongpu Liang**[1], **Ju Jiao**[5], **Zongheng Zheng**[1], **Jiafeng Fang**[1], **Purun Lei**[1], **Josbert M Metselaar**[2], **Gert Storm**[4,5], **Wim E Hennink**[4], **Fabian Kiessling**[2,6], **Hongbo Wei**[1,‡], **Twan Lammers**[2,4,5,‡], **Yang Shi**[2,‡], **Bo Wei**[1,‡]

[1]Department of Gastrointestinal Surgery, the Third Affiliated Hospital of Sun Yat-sen University, Guangzhou 510630, China

[2]Institute for Experimental Molecular Imaging, Uniklinik RWTH Aachen and Helmholtz Institute for Biomedical Engineering, Faculty of Medicine, RWTH Aachen University, 52074 Aachen, Germany

[3]Vascular Biology Research Institute, School of Basic Course, Guangdong Pharmaceutical University, Guangzhou 510006, China

[4]Central Laboratory, the Third Affiliated Hospital of Sun Yat-sen University, Guangzhou 510630, China, Department of Pharmaceutics, Utrecht Institute for Pharmaceutical Sciences, Utrecht University, 3584 CG Utrecht, The Netherlands

[5]Department of Nuclear Medicine, the Third Affiliated Hospital of Sun Yat-sen University, Guangzhou 510630, China, Department of Targeted Therapeutics, MIRA Institute for Biomedical Technology and Technical Medicine, University of Twente, 7500 AE Enschede, The Netherlands

[6]Fraunhofer MEVIS, Institute for Medical Image Computing, 52074 Aachen, Germany

[#] These authors contributed equally to this work.

Abstract

Gastrointestinal (GI) cancers are among the most lethal malignancies. The treatment of advanced-stage GI cancer involves standard chemotherapeutic drugs, such as docetaxel, as well as targeted therapeutics and immunomodulatory agents, all of which are only moderately effective. We here show that Π electron-stabilized polymeric micelles based on PEG-*b*-p(HPMAm-Bz) can be loaded highly efficiently with docetaxel (loading capacity up to 23 wt%) and potentiate chemotherapy responses in multiple advanced-stage GI cancer mouse models. Complete cures and full tumor regression were achieved upon intravenously administering micellar docetaxel in subcutaneous gastric cancer cell line-derived xenografts (CDX), as well as in CDX models with intraperitoneal and lung metastases. Nanoformulated docetaxel also outperformed conventional docetaxel in

[‡] Corresponding authors: Hongbo Wei: weihb@mail.sysu.edu.cn Twan Lammers: tlammers@ukaachen.de Yang Shi: yshi@ukaachen.de Bo Wei: weibo3@mail.sysu.edu.cn.

Author contributions: C.H.L., X.Y.B., and C.L.Q. contributed equally to this work. B.W., Y.S., T.L., and H.B.W. designed the research. C.H.L., X.Y.B., C.L.Q., Q.X.S., X.Y.H., T.Y.L., H.B.Z., X.M.Z., R.P.L., J.J., Z.H.Z., J.F.F., and P.R.L. performed the experiments. C.H.L., B.W., Y.S., and T.L. and analyzed the data. B.W., Y.S., T.L., and C.H.L. wrote the paper. Y.S., T.L., B.W., F.K., W.E.H., G.S. and H.B.W. revised the manuscript. All authors read and approved the submitted manuscript.

Notes: The authors declare no competing financial interest.

Europe PMC Funders Author Manuscripts

a patient-derived xenograft (PDX) model, doubling the extent of tumor growth inhibition. Mechanistically, micellar docetaxel modulated the tumor immune microenvironment in CDX and PDX tumors, increasing the ratio between M1- and M2-like macrophages, and toxicologically, it was found to be very well-tolerated. These findings demonstrate that Π-conjugated polymeric micelles loaded with docetaxel hold significant potential for the treatment of advanced-stage GI cancers.

Keywords

Nanomedicine; Polymeric micelles; Gastrointestinal cancer; Tumor targeting; Taxane therapy; Tumor Microenvironment

Introduction

Gastrointestinal (GI) cancers are among the most frequent malignancies, causing more than a million deaths in 2018.[1] There are no good treatment options for advanced-stage GI cancers, and the efficacy of standard chemotherapy, molecularly targeted therapy and immunotherapy is relatively low. Efficacious drug treatment of GI cancers is furthermore complicated by the fact that only a relatively small portion of patients qualify for molecularly targeted therapeutics and/or immunotherapy[2,3] As a result of this, advanced-stage GI cancer therapy is typically based on the use of standard chemotherapeutic drug, most prominently docetaxel (DTX).[4,5] It is known, however, that taxane-based chemotherapeutic treatments are only rarely curative,[6] and that their use almost always entails the development of severe side effects.[7]

Nanomedicine formulations can improve the efficacy and reduce the toxicity of chemotherapeutic drugs.[8–10] Nanomedicine-based drug targeting to tumors traditionally relies on two main mechanisms, i.e. passive targeting via the so-called enhanced permeability and retention (EPR) effect[11,12] and active targeting via the use of ligands recognizing receptors overexpressed at the pathological site.[13,14] Both strategies have shown significant potential in preclinical studies.[8,15,16] At the clinical level, however, most cancer nanomedicines have thus far failed to achieve significantly improved response rates and survival times in large cohorts of patients.[17] This notion has recently sparked an intense debate on the value of nanomedicine-based tumor targeting.[17–21] This controversy has contributed to the realization that we have to move on from a “nanoformulation-first” approach towards a more comprehensive disease-driven approach, considering besides rational nanomedicine design also key translational issues such as patient stratification and combination therapies.[8,19,20,22–25]

A crucial element to promote nanomedicine translation is the use of advanced and more predictive mouse models for in vivo efficacy evaluation. More relevant models include metastatic, genetically engineered and patient-derived models, which have all demonstrated benefits in cancer drug development as compared to conventional subcutaneous tumors.[26,27]. For example, the value of patient-derived xenografts (PDX) has recently been demonstrated in a large study in which 62 drug treatments were tested in ~1000 PDX models, showing that that patient-derived models predicted clinical responses more accurately than conventional

Europe PMC Funders Author Manuscripts

tumor models. Furthermore, they are also valuable for identifying biomarkers to stratify responders from non-responders.[28]

We here employed multiple advanced mouse models to explore docetaxel (DTX) - based nanotherapy for the treatment of advanced-stage GI cancer. To this end, we formulated DTX in Π electron-stabilized polymeric micelles (DTX-PM), which are highly stable and which can be efficiently loaded with drugs containing aromatic groups via Π-Π stacking interactions in the micellar core.[29] The potential of DTX-PM was demonstrated in a variety of advanced-stage GI cancer models.

Results

Preparation and characterization of docetaxel-containing polymeric micelles

Π electron-stabilized polymeric micelles based on methoxy poly(ethylene glycol)-b-(N-(2-benzoyloxypropyl)methacrylamide) (mPEG-b-p(HPMAm-Bz)) were used for DTX loading and targeting (Figure S1, molecular weight by gel permeation chromatography (GPC) was 22 kDa and the polydispersity index was 1.7, molecular weight by proton nuclear magnetic resonance was 21 kDa, corresponding to 65 repeating units, methods as reported ref.[29]). These micelles can efficiently and stably encapsulate anticancer agents in their hydrophobic cores via Π-Π stacking and hydrophobic interactions between the aromatic groups of the polymer chains and those of drug molecules[29,30] (Figure 1A-B). DTX was loaded in the Π electron-stabilized micelles using the nanoprecipitation method (Figure 1A-B). The resulting DTX-PM showed very high encapsulation efficiency and loading capacity (maximum EE = 85% and maximum LC = 23 wt%, respectively; Figure 1C). The average diameter of the PM was 70-110 nm, depending on the feed ratio of DTX (Figure 1D). The zeta potential of the DTX-PM was 0±1 mV (Figure S2). The size distribution was narrow for all formulations, as evidenced by DLS analysis (PDI = 0.1; Figure 1D). TEM images of the micelles showed relatively homogenous size distribution and spherical morphology of the micelle particles (Figure 1E). DTX release from the micelles was assessed under sink conditions using dialysis bags,[31] which showed sustained slow release behavior of micelles (~50% in 24 hours and ~60% in 96 hours) while 90% of free drug leaked out via the dialysis bag in 2 hours. In addition, both empty and DTX-PM were stable for at least 96 hours at pH 7.4 and 37 °C (Figure S3). These findings demonstrate that DTX-loaded Π electron-stabilized polymeric micelles have suitable pharmaceutical and physicochemical properties for in vivo drug delivery.

Performance of DTX-PM in GI cancer cell lines

The in vitro cytotoxicity of DTX-PM was studied in SGC7901 human gastric cancer cells and HCT116 human colorectal carcinoma cells. The results Figure 1G-H indicate that DTX-PM was equally efficient as free DTX in inhibiting GI cancer cell growth in vitro. The IC50 values of DTX-PM in SGC7901 and HCT116 cells were 8 and 42 μM respectively, as compared to 6 and 40 μM for free DTX, respectively. We next assessed apoptosis induction and cell cycle arrest in response to DTX-PM, free DTX and empty PM (Figure S4). The percentages of cells undergoing apoptosis were similar for DTX-PM and free DTX, with values of 25 and 20% in SGC7901 cells, and 24 and 22% in HCT116 cells, respectively

(Figure 1I-J). Taxane drugs, such as DTX, exert their pharmacological effect via stabilizing microtubuli, preventing cells from dividing and thus arresting them in G2/M. Cell cycle analysis showed that both DTX-PM and free DTX prominently induced mitosis inhibition and G2/M arrest, with values of 37 and 41% in SGC7901 cells, and 71 and 56% in HCT116 cells, respectively (Figure 1K and L, and Figure S4). Importantly, apoptosis induction and cell cycle arrest were negligible for empty PM, confirming their cytocompatibility.29 GI cancers often metastasize, resulting in disease recurrence and morbidity.[32,33] To study metastasis inhibition in vitro, we performed transwell assays with SGC7901, investigating the ability of DTX-PM and free DTX to block cell migration and invasion through Matrigel-coated membranes (Figure S5).[34] As shown in Figure 1M-N, both free DTX and DTX-PM efficiently suppressed migration and invasion, by 70 and 90% for free DTX, and by 75 and 85% for DTX-PM, respectively. These cell culture experiments demonstrate that free DTX and DTX-PM have a similar mechanism of action (G2/M arrest, apoptosis induction) and are equally effective in vitro in terms of inhibiting cell growth, migration and invasion.

Cell line- and patient-derived mouse models for advanced-stage GI cancer

We established multiple mouse models to study the in vivo performance of DTX-PM in advanced-stage GI cancer. These include cell-line derived xenografts (CDX) as well as patient-derived xenografts (PDX) derived from an advanced-stage colorectal cancer patient. CDX were established by inoculating SGC7901 human gastric cancer cells subcutaneously (s.c.), and by injecting them intraperitoneally (i.p.) and intravenously (i.v.). Correspondingly, mice developed subcutaneous tumors, peritoneal and lung metastases (Figure 2A). These locations represent clinically relevant sites for metastatic spread in case of advanced-stage GI cancer.[35–38] The PDX model was established by subcutaneously implanting tumor tissue obtained from a colorectal cancer patient in mice (referred to as generation 0; G0), and by subsequently transplanting parts of this tumor into the next generation of mice (G1) (Figure 2B). Histopathological and immunofluorescence analyses showed that G0 and G1 PDX tumors had a similar phenotype as the original patient tumor with regard to vascularization, fibroblast and tumor-associated macrophage (TAM) content (Figure 2C and S6). Interestingly, however, the collagen content was significantly higher in the original patient tumor than in the G0 and G1 PDX tumors (Figure 2C and S6). We also compared the microenvironmental make-up of PDX tumors to that of CDX tumors. The microvessel density (MVD) and the collagen content were both found to be more than a two-fold higher in the CDX model (Figure 2D-F). The CDX model furthermore presented with a higher TAM density and with a higher ratio of M1-like TAM vs. M2-like TAM (Figure 2D-G). These notions exemplify the differential microenvironmental make-up of different tumor models, and they underline the importance of studying nanomedicine efficacy in multiple models when aiming to properly capture their therapeutic potential.

Antitumor efficacy of DTX-PM in the subcutaneous CDX model

Initially, the subcutaneous CDX model, based on inoculated SGC7901 cells, was used to evaluate DTX-PM-based nanotherapy. In this model, 15 mg/kg DTX induced significant body weight loss, and therefore two lower doses (10 and 5 mg/kg) were chosen, with a dosing schedule similar as previously reported.[29] Treatments were applied when the tumors reached a volume of ~50 mm^3. The formulations were injected intravenously every 3 days,

for a total of 5 injections. Mice treated with PBS showed rapid tumor growth, reaching ~800 mm^3 within two weeks (Figure 3A). Tumor growth was slightly inhibited by free DTX administered at 5 and 10 mg/kg. The efficacy of DTX-PM was significantly higher at both doses as compared to free DTX (Figure 3A). DTX-PM at 10 mg/kg exhibited the best efficacy and near complete tumor regression was achieved, while free DTX at the same dose was clearly less effective (Figure 3B). The therapeutic efficacy of the formulations was confirmed via ex vivo tumor size and weight analysis (Figure 3C and D). Thus, DTX-PM at 10 mg/kg appeared to be a highly potent regimen for treating this CDX model of GI cancer. The efficacy of the DTX-PM formulation was verified via histochemical analysis of tumors harvested on day 16 after the first injection (Figure S7). The proliferation index was analyzed by Ki67 staining and apoptosis induction was assessed via quantifying by the expression of cleaved caspase 3. As shown in Figure 3E, the proliferation index was significantly reduced upon treatment with 10 mg/kg DTX-PM. Furthermore, 10 mg/kg of DTX-PM was more effective than 10 mg/kg of free DTX in inducing apoptosis (Figure 3F). Overall, the high potency of DTX-PM was likely resulted from the significantly prolonged blood circulation ($t_{1/2}$=13.6 hours, Figure S8), which is of crucial importance for tumor targeting by nanoparticles via the EPR effect.[22,25]

Apart from the antitumor effect of DTX-PM, its ability to modulate the tumor immune microenvironment (TIME)[39] was investigated. Taxanes, including DTX, have been shown to change the polarisation of macrophages towards an M1-like phenotype.[40,41] Cancer models established in athymic nude mice have a largely preserved innate immune system, which includes TAM.[42] TAM phenotype was analyzed by immunofluorescence staining to identify M1-like and M2-like macrophages (Figure 3G and S9). As compared to controls, the ratio between M1-like and M2-like TAM roughly doubled upon the use of 5 mg/kg of free DTX and DTX-PM, and it increased by almost a 3-fold upon the use of 10 mg/kg DTX-PM (Figure 3H). The findings indicate that DTX nanoformulations more potently modulate the TIME than DTX in free from.

Safety assessment is crucial when developing cancer nanomedicines. Mice treated with both doses of DTX-PM did not suffer from significant body weight loss (Figure S10). Clinical chemistry analyses of blood samples showed that that DTX-PM treatment did not alter the levels of alanine aminotransferase (ALT), aspartate aminotransferase (AST) and serum creatinine (SCr), demonstrating lack of liver toxicity.[43] (Figure S11). Notably, one mouse treated with 5 mg/kg of free DTX presented with obviously increased levels of ALT and AST (Figure S11). In addition to this, complete blood count analysis showed that there was no significance difference between the five groups with regard to the number of red blood cells (RBC), white blood cells (WBC) and platelets (PLT) (Figure S11). Furthermore, H&E staining of all major organs was performed, showing that neither free DTX nor DTX-PM induced severe organ damage (Figure S11). Collectively, these findings confirm the biocompatibility of DTX-PM.

Efficacy of DTX-PM in CDX-based peritoneal and lung metastasis models

The potential of DTX-PM as compared to free DTX was subsequently evaluated in two SGC7901-based CDX metastatic models of advanced-stage GI cancer, colonizing the

peritoneal cavity and the lungs (Figure 2). To this end, free and micellar DTX were intravenously administered at 5 and 10 mg/kg, every 4 days for a maximum of five treatments. In the abdominal metastasis model, 18F-FDG-enhanced PET-CT imaging clearly showed a lower metastatic burden in the peritoneal cavity at day 16 after four treatments with DTX-PM as compared to free DTX and PBS control (Figure 4A). In line with this, the average survival time of mice treated with PBS, free DTX administered at 5 and 10 mg/kg and DTX-PM administered at 5 mg/kg were 57, 59, 74 and 147 days, respectively. At the end of the study, at day 210, 5 out of 6 mice in the 10 mg/kg DTX-PM were still alive, as compared to 1 out of 6 in the 5 mg/kg DTX-PM group, and to 0 out of 6 for mice treated with PBS and with free DTX (Figure 4B). In a second study with peritoneal SGC7901-based CDX metastases, mice were treated similarly but sacrificed at day 21 after the first treatment. By means of abdominal anatomy examination, it was found that the number of intraperitoneal nodules in the DTX and DTX-PM groups was substantially lower than that in the PBS group (Figure 4C and E-I). Furthermore, DTX-PM was found to be significantly more effective than DTX at 5 mg/kg (Figure 4C).

A third metastatic CDX model of advanced-stage GI cancer was established via the i.v. injection of SGC7901 cells, resulting in nodules in the lungs. Free and DTX-PM were again administered at a dose of 5 and 10 mg/kg, every 4 days and for a maximum of five treatments. As shown in Figure 4D and 4J-N, the number of lung nodules was significantly reduced for both free DTX and DTX-PM as compared to the PBS-treated control group. Furthermore, DTX-PM was more effective than free DTX (Figure 4D). In the 10 mg/kg DTX-PM group, the number of metastatic nodules was significantly lower than that in the 10 mg/kg free DTX group. In both metastasis models, we also assessed the safety of DTX-PM treatment. In line with the above observations, no significant body weight loss was observed, confirming the safety of the formulation (Figure S10).

Antitumor efficacy of DTX-PM in a patient-derived GI cancer model

The efficacy of DTX-PM was finally also evaluated using a patient-derived xenograft (PDX) model. PDX models have been shown to better mimic patient tumors than cancer cell line-derived models and they more realistically reflect the clinical response to drug treatments.[28,44,45] The treatments were given every 4 days for in total 5 times after the tumors were palpable. In the PDX model, PBS-treated control tumors reached an average volume of 800 mm3 within three weeks (Figure 5A). Tumor growth was inhibited by five injections of free DTX (injected every four days at 10 mg/kg). DTX-PM significantly improved antitumor efficacy as compared to free DTX ($P < 0.05$). The higher efficacy of DTX-PM compared to free DTX was confirmed by determining the weights of excised tumors (Figure 5B). DTX-PM also significantly enhanced apoptosis induction and reduced proliferation as compared to free DTX, as assessed by cleaved caspase 3 and Ki67 staining (Figure 5C-E). To exemplify the efficacy benefit of DTX-PM over free DTX, individual tumor growth curves are plotted in Figure 5F-G. In the free DTX group, all mice presented with continuous tumor growth during treatment. In the DTX-PM group, the growth rate was slower than the DTX group and complete growth inhibition was achieved 2 out of 6 mice.

Since DTX-PM effectively modulated the TIME via affecting TAM polarization in the CDX model, we also studied this in the PDX model. As shown in Figure 5H and 5I, both DTX and DTX-PM increased the ratio of M1-like to M2-like TAM, but this effect as significantly stronger for DTX-PM. Moreover, also in this study setup, mice did not experience obvious body weight loss after repeated injections of DTX-PM (Figure S10).

Discussion

We here demonstrate that Π electron-stabilized polymeric micelles can potentiate the efficacy of DTX in multiple advanced-stage GI cancer models. The results obtained indicate that this micellar taxane formulation holds potential for clinical translation.

Traditionally, nanomedicines are only tested in conventional subcutaneous cell-line derived xenograft (CDX) models. It is known that such CDX models poorly predict the potential of drugs and drug delivery systems. The results presented here show that DTX entrapped in Π electron-stabilized polymeric micelles significantly improves the therapeutic efficacy of DTX in subcutaneous CDX tumors, in two different CDX-based metastatic models and in a patient-derived xenograft (PDX) model of advanced-stage colorectal cancer. As compared to free DTX, the DTX-loaded Π electron-stabilized micelles induced multiple complete cures and they potently prolonged survival times, underlining the potential of DTX-PM for GI cancer therapy.

In addition to the direct tumor cell killing effects of the nanoformulation, we observed that the Π electron-stabilized DTX micelles modulated the polarization of tumor-associated macrophages (TAM), much stronger than free DTX, which was likely due to that TAMs are highly active in taking up nanomedicines accumulated in tumors as reported by other groups.[46] This effect is important in the context of immunotherapy priming.[47–50] Nanomedicines with TAM modulating effects have been reported before, based e.g. on polymeric nanoparticles containing Toll-like receptor 7/8 agonists, as well as on inorganic iron oxide-based nanoparticles with intrinsic capabilities to affect TAM polarization.[51–53] DTX-PM differ from these nanoformulations in the sense that they contain a clinically well established and routinely used anti-GI cancer drug.

The developed DTX nanoformulation relies on Π electron-stabilized polymeric micelles with physical interactions between the aromatic groups of the polymer and the drug payload. This ensures proper in vivo stability, and promotes efficient drug loading and retention. Several taxane-based nanomedicine formulations have been evaluated clinically, including Abraxane, Genexol, NK105, BIND-014 and CriPec.[24,54] Our Π electron-stabilized polymeric micelle platform extends these previous developments because it enables efficient tumor targeting and therapy upon using simple and straightforward preparation and formulation procedures, including avoidance of chemical modification of the drug payload.

When aiming to translate cancer nanomedicines to the clinic, it is important to test their efficacy and safety in multiple relevant and realistic preclinical models.[55–58] In this context, we have to keep in mind that clinical responses will be heterogeneous, especially in the advanced-stage patients that are typically included in phase I and phase II clinical

trials. In line with this notion, our findings show that the efficacy of DTX loaded in Π electron-stabilized polymeric micelles is lower in patient-derived tumors than in cell-line derived models. Nanoformulated DTX remains to be significantly superior as compared to free DTX, but the number of complete cures is reduced, and the responses are more heterogeneous. Because of these differential responses, and particularly also because of differences related to the extent of the EPR effect in different patients and tumors, it will be crucial to come up with materials and methods for patient stratification in cancer nanomedicine clinical trials, in order to help preselect those individuals most likely to respond, and to exclude those unlikely to respond from clinical trials.[8,25,58,59]

Conclusion

Taking everything together, we here describe the development and testing of a novel docetaxel-containing nanomedicine formulation for the treatment of high-medical need GI cancers. The Π electron-stabilized micellar nanodrug induced prominent therapeutic effects, including complete cures, in multiple different GI cancer models in mice, and it outperformed free DTX in all four models evaluated. Apart from direct tumor cell killing, micellar DTX also modulated the polarization of macrophages in the tumor immune microenvironment, and it was found to be very well-tolerated. These findings exemplify the potential of Π electron-stabilized polymeric micelles for anticancer drug delivery, and they indicate that docetaxel-loaded Π electron-stabilized micelles may be valuable for improving the treatment of advanced-stage GI cancers.

Materials and Methods

Materials

PEG-*b*-p(HPMAm-Bz) was synthesized and characterized using previously established protocols.[29] Docetaxel (DTX, purity >98%) was purchased from Haoxuan Biotech Co. Ltd. (Xi'an, China). DTX injection formulation was provided by Hengrui Medicine Co. Ltd. (Jiangsu, China). CCK8 kit and the Annexin V-FITC apoptosis detection kit were purchased from KeyGEN Biotech Co. Ltd. (Jiangsu, China). The cell cycle analysis kit was obtained from 4A Biotech Co. Ltd. (Beijing, China). Fetal bovine serum (FBS) and the cell culture medium RPMI-1640 were obtained from Yongjin Biotech Co. Ltd. (Guangzhou, China). Trypsin and phosphate buffer saline were obtained from Xiangbo Biotech Co. Ltd. (Guangzhou, China).

Cell lines

SGC7901 was a kind gift from Dr. Lipu Xu at the Cancer Center, Sun Yat-Sen University, China. HCT116 was purchased from Zhong Qiao Xin Zhou Biotechnology Co. Ltd. (Shanghai, China).

Animals

BALB/C nude mice were purchased from Guangdong Medical Laboratory Animal Center (Guangzhou, China). The animals were used in the present study under the guidelines of the Animal Experimental Ethics Committee of Guangdong Pharmaceutical University, China

Europe PMC Funders Author Manuscripts

(reference number: gdpulac2016027). For the pharmacokinetics and biodistribution study, BALB/cAnNRj female mice were ordered from Janvier Labs, France, and the study was conducted upon the approval by local and institutional ethical committees.

Patient specimens

Patient tumor tissues were obtained during operation with informed consent and the research was approved from the Third Affiliated Hospital Ethics Committee of Sun Yat-sen University. The tissue samples were used according to relevant national and international guidelines.

DTX-PM preparation

DTX-PM were prepared using a nano-precipitation method as previously reported.[29] Briefly, DTX and PEG-b-p(HPMAm-Bz) were dissolved in tetrahydrofuran (THF) after gentle mixing. The mixture in THF was added dropwise in ultrapure water under vigorous stirring, followed by evaporation of THF at room temperature for 48 hours. The resulted formulation was filtrated through a 0.22 μm nylon membrane.

DTX-PM characterization

The size and zeta potential of DTX-PM were measured by Zetasizer Nano ZS90 (Malvern, UK). Each sample was measured 3 times of 12 runs. The morphology of DTX-PM was observed assessed using a transmission electron microscope (HT7700, Hitachi, Japan) after the samples were diluted 10 times by distilled deionized water. To detect the loading content of DTX in DTX-PM, the micelle formulations were diluted 10 time with acetonitrile and vigorously mixed to dissolve the micelles. The concentration of DTX was detected by HPLC analysis (LC-20AT, Shimadzu, Japan). The standard curve was obtained using a series standard concentration of DTX from 25-200 μg/mL. Encapsulation efficiency (EE) and loading capacity (LC) were calculated according to the following formulas:

$$\mathrm{LC}(\%) = \frac{\text{Weight of DTX in nanopartic les}}{\text{Weight of nanopartic les}} \times 100\%$$

$$\mathrm{EE}(\%) = \frac{\text{Weight of DTX in nanopartic les}}{\text{Weight of DTX added}} \times 100\%$$

Cell culture

The SGC7901 and HCT116 cells were cultured using 1640 medium (GIBCO), supplemented with 10% of fetal bovine serum (FBS, GIBCO). The cells were incubated at 37 °C in an incubator with 5% CO_2. Cells were passed every 2 or 3 days when the flasks were 75% confluent.

Cell viability assay

SGC7901 and HCT116 cells were seeded in 96-well plates with 3,000 cells per well. After 24 hours of incubation, the medium was refreshed and free DTX, DTX-PM (~6 wt% of LC) and the PM vehicle were added to the cells, followed by incubation at 37 °C with 5% CO_2 for 72 hours. After incubation, each well was added with 10 μL CCK8 reagent, and then the plates were incubated at 37 °C for 4 hours. The absorbance was measured at 450 nm

by a microplate reader (ELX800, Biotek, USA). The cell viability was calculated with cells incubated in the medium as control.

Apoptosis assay

SGC7901 and HCT116 cells were cultured in 6-well plates with 50,000 cells per well. After incubation for 24 hours, free DTX and DTX-PM at IC50 in each cell line were added to the cells, and the PM vehicle with concentrations corresponding to those in the DTX-PM samples were tested. The cells were incubated with the samples for 24 hours and then harvested, stained with the apoptosis kit, and analyzed by flow cytometry (FACSCanto II, BD, USA).

Cell cycle arrest assay

The cells were cultured and treated as described in the apoptosis assay. The cells were incubated with DTX-PM and DTX at IC50 for 24 hours, and were harvested and fixed using 75% ethanol at 4 °C for 18 hours. Subsequently, cells were incubated with 0.4mL of PI in cell cycle staining buffer (contained 15 μL PI solution and 4 μL DNase-free RNase) at 37 °C for 30 minutes. The detection was performed by flow cytometry (FACSCanto II, BD, USA). The data were analyzed by the software LT (BD Biosciences).

Cell migration assay

SGC7901 cells were cultured in 6-well plates. After incubation for 24 hours, DTX, DTX-PM at IC50 and the corresponding concentration of PM vehicle were added the wells. The cells were incubated with the samples for 6 hours, and then harvested and resuspended at a density of 106/mL in serum-free medium. 100 μL of cell suspensions were added to transwells and incubated for 48 hours. Afterwards, the cells were fixed with 4% paraformaldehyde and stained with 1% crystal violet (w/v, prepared in PBS). Cells remained on the upper chamber were wiped gently. The migrant cells on the bottom side of the transwells were counted in five representative images via microscope.

Cell invasion assay

The experimental procedure was identical to that of the cell migration assay, apart from that the transwells were pre-coated with 60 μL of Matrigel before using.

Hematoxylin and eosin (HE) staining

Tissues were fixed with 4% paraformaldehyde, dehydrated in ethanol, embedded in paraffin, and then cut into 3μm slices. The tissue slices were dewaxed and rehydrated, and then stained with hematoxylin and eosin. The morphology of tissues was observed under an orthopedic microscope (BX51, Olympus, Japan).

Sirius red staining

Sirius red staining was used for the observation of collagen. Tissue sections were dewaxed and rehydrated, and incubated with Sirius red. Images were obtained under an orthopedic microscope

Immunohistochemistry

Tissue sections were prepared as mentioned above and immunohistochemistry was performed according to the standard operating procedure. In brief, slices were deparaffinized in xylene, dehydrated in gradient ethanol, and treated with microwave for antigen retrieval. Then, the sections were pre-incubated in 3% hydrogen peroxide in methanol at room temperature for 10 minutes, blocked with 10% bovine serum albumin (BSA) and incubated with the primary antibodies (1:100 dilution for Ki67, cat.No. ab15580, Abcam; 1:100 dilution for CD31, cat.No. EP3095, Abcam; 1:100 dilution for Caspase 3, cat.No. BF0711, Affinity) overnight at 4 °C. Afterwards, the tissue slices were incubated with an HRP-conjugated secondary antibodies, stained with DAB and counterstained with hematoxylin. Images were obtained under a microscope in a 400×field and five representative fields were quantified using the software IPP 6.0 and assessed by two individual investigators. To analyze the cell proliferation, the number of Ki67 positive/proliferating cells (nuclei stained brown) were divided by the total number of cells in a field to calculate the proliferating index.[60]

Immunofluorescence

Frozen sections were used for immunofluorescence analysis. Tumor tissue sections were defrosted for 10 min in deionized water and treated with microwave for antigen retrieval. Then, sections were incubated with 10% BSA for 1 h at room temperature and incubated with primary antibody (1:500 dilution for CD11b, cat.No. Ab204471, Abcam; 1:100 dilution for α-SMA, cat.No. 53-9760-80, Thermo Fisher; 1:100 dilution for Caspase 3; cat.No. BF0711; Affinity, 1:100 dilution for CD86, cat.No.ab239057, Abcam; 1:100 dilution for CD206, cat.No. Ab8918, Abcam) at 4 °C overnight. Afterwards, the sections were incubated with fluorophore-labeled secondary antibody for 1 h, followed by DAPI staining. Fluorescence were observed under a laser scanning confocal microscope or fluorescence microscope at 400× magnification. The relative expression of cleaved caspase 3 was calculated by comparing the integrated optical density (IOD) value of the area stained brown of treated groups to that of the PBS control group using IPP software.[61]

Subcutaneous models

The subcutaneous SGC7901 model was established and used as described above in female BALB/C nude mice. The mice were enrolled in the study when the tumor size reached ~50-100 mm^3. The mice were divided into 5 groups, which were treated with PBS, 5 mg/kg DTX or DTX-PM, and 10 mg/kg DTX or DTX-PM (PM with ~6.5 wt% of LC). The mice were treated every 3 days for in total 5 times. Tumor volume and body weight of mice were monitored. The blood, tumors and major organs of the mice were harvested after sacrificing for further analysis. For pharmacokinetics and distribution study, 1×10^6 CT26 cancer cells were inoculated and the mice were used when the tumor size reached ~10 mm diameter. The mice received DTX-PM or free DTX at 10 mg/kg, blood and organs samples were collected at different time point and were processed according to previously established protocols.[29] The concentrations of DTX in the samples were analyzed by HPLC (mobile phase: ACN/water=4/6 with 0.1% trifluoroacetic acid, detection wavelength at 230 nm, flow

rat at 0.8 mL/min, column: ACQUITY UPLC BEH C18 Column, 130Å, 1.7 μm, 2.1 mm X 50 mm).

Peritoneal metastasis model

To evaluate the therapeutic efficacy of DTX-PM in the peritoneal metastasis model, female BALB/c nude mice were intraperitoneally inoculated with 5×10^6 SGC7901 cells per mice. The mice were randomly divided into 5 groups 10 days post inoculation, 6 mice per group, which were administered with PBS, 5 mg/kg DTX or DTX-PM, and 10 mg/kg DTX or DTX-PM. The treatments were given every 4 days for a total of 5 times. Tumor nodes exceeding 0.5 mm in diameter in the abdominal cavity were recorded.

Lung metastasis model

BALB/c nude mice were injected with SGC7901 cells (5×106 cells per mice) via the tail vein. After 10 days of inoculation, a total of 30 mice were divided into 5 groups treated with PBS, 5 mg/kg DTX or DTX-PM, and 10 mg/kg DTX or DTX-PM. The treatments were given every 4 days and a total of 5 times. The lungs were prepared in histology slices and HE staining of the tissue slices was performed. The lung sections were imaged under fluorescence microscopy to record the number of intrapulmonary micrometastases.

Patient-derived xenograft (PDX) model

Fresh tumor tissues were obtained from a colorectal cancer patient during operation. Tumor tissues of around 3 mm^3 in diameter were subcutaneously transplanted in the right flanks of BALB/c mice (denoted as G0). When the tumor size in G0 mice reached ~ 500 mm^3, the tumors were harvested and sliced into $3\times3\times3$ mm^3 fragments and were subcutaneously inoculated into another BALB/c nude mice which were denoted as G1.

Statistical analysis

Quantitative data were statistically described by means ± standard deviation. Differences between the groups were assessed by Student's t-test (two groups) or one-way ANOVA (multiple groups). A p-value <0.05 was considered to represent statistical significance.

Supplementary Material

Refer to Web version on PubMed Central for supplementary material.

Acknowledgements

The authors gratefully acknowledge Liuming He and Rui Guo (Department of Biomedical Engineering, Ji'nan University), and Guohui Wan (School of Pharmaceutical Sciences, Sun Yat-sen University) for helpful discussions. SGC7901 cells were kindly donated by Dr. Lipu Xu at the Cancer Center, Sun Yat-sen University, China.

Funding

This work was supported by grants from Science and Technology Planning Project of Guangdong Province (2017B020227009 and 2017A010103009), by Fundamental Research Funds for the Central Universities (16ykjc23), by the National Natural Science Foundation of China (81472825 and 81773095), by the Outstanding Young Talents Support Program of the Third Affiliated Hospital of Sun Yat-sen University, by the China Scholarship Council (CSC), by the European Research Council (ERC: Starting Grant NeoNaNo (309495) and Proof-of-Concept Grant PIcelles (813086)), by German Research Foundation (DFG: GRK/RTG 2375: Tumor-

Europe PMC Funders Author Manuscripts

targeted Drug Delivery (331065168)), and by the Aachen Interdisciplinary Center for Clinical Research (IZKF; Project O3-2).

Data availability

The raw/processed data are available upon reasonable request.

References

(1). Bray F, Ferlay J, Soerjomataram l, Siegel RL, Torre LA, Jemal AA. Global cancer statistics 2018: GLOBOCAN estimates of incidence and mortality worldwide for 36 cancers in 185 countries. CA Cancer J Clin. 2018; 68 :394–424. [PubMed: 30207593]

(2). Ratti M, Lampis A, Hahne JC, Passalacqua R, Valeri N. Microsatellite instability in gastric cancer: molecular bases, clinical perspectives, and new treatment approaches. Cell Mol Life Sci. 2018; 75 :4151–4162. [PubMed: 30173350]

(3). Muro K, Chung HC, Shankaran V, Geva R, Catenacci D, Gupta S, Eder JP, Golan T, Le DT, Burtness B. Pembrolizumab for patients with PD-L1-positive advanced gastric cancer (KEYNOTE-012): a multicentre, open-label, phase 1b trial. Lancet Oncol. 2016; 17 :717–726. [PubMed: 27157491]

(4). Ajani JA. Evolving chemotherapy for advanced gastric cancer. Oncologist. 2005; 10 :49–58. [PubMed: 16368871]

(5). Nishiyama M, Wada S. Docetaxel: its role in current and future treatments for advanced gastric cancer. Gastric cancer. 2009; 12 :132–141. [PubMed: 19890692]

(6). Bernards N, Creemers G, Nieuwenhuijzen G, Bosscha K, Pruijt J, Lemmens V. No improvement in median survival for patients with metastatic gastric cancer despite increased use of chemotherapy. Ann Oncol. 2013; 24 :3056–3060. [PubMed: 24121120]

(7). Al-Batran S-E, Hozaeel W, Tauchert F, Hofheinz R-D, Hinke A, Windemuth-Kieselbach C, Hübner A, Burmester M, Koenigsmann M, Wiegand J. The impact of docetaxel-related toxicities on health-related quality of life in patients with metastatic cancer (QoliTax). Ann Oncol. 2015; 26 :1244–1248. [PubMed: 25755108]

(8). Shi J, Kantoff PW, Wooster R, Farokhzad OC. Cancer nanomedicine: progress, challenges and opportunities. Nat Rev Cancer. 2017; 17 :20. [PubMed: 27834398]

(9). Kataoka K, Harada A, Nagasaki Y. Block copolymer micelles for drug delivery: design, characterization and biological significance. Adv Drug Deliv Rev. 2012; 64 :37–48.

(10). Kwon GS, Kataoka K. Block copolymer micelles as long-circulating drug vehicles. Adv Drug Deliv Rev. 2012; 64 :237–245.

(11). Gerlowski LE, Jain RK. Microvascular permeability of normal and neoplastic tissues. Microvasc Res. 1986; 31 :288–305. [PubMed: 2423854]

(12). Matsumura Y, Maeda H. A new concept for macromolecular therapeutics in cancer chemotherapy: mechanism of tumoritropic accumulation of proteins and the antitumor agent smancs. Cancer Res. 1986; 46 :6387–6392. [PubMed: 2946403]

(13). Zhong Y, Meng F, Deng C, Zhong Z. Ligand-directed active tumor-targeting polymeric nanoparticles for cancer chemotherapy. Biomacromolecules. 2014; 15 :1955–1969. [PubMed: 24798476]

(14). Mi P, Cabral H, Kataoka K. Ligand-Installed Nanocarriers toward Precision Therapy. Adv Mater. 2019 1902604

(15). Van der Meel R, Lammers T, Hennink WE. Cancer nanomedicines: oversold or underappreciated? Expert Opin Drug Deliv. 2017; 14 :1–5. [PubMed: 27852113]

(16). Anselmo AC, Mitragotri S. Nanoparticles in the clinic: An update. Bioeng Transl Med. 2019; 4 e10143 [PubMed: 31572799]

(17). Danhier F. To exploit the tumor microenvironment: since the EPR effect fails in the clinic, what is the future of nanomedicine? J Control Release. 2016; 244 :108–121. [PubMed: 27871992]

(18). Wilhelm S, Tavares AJ, Dai Q, Ohta S, Audet J, Dvorak HF, Chan WC. Analysis of nanoparticle delivery to tumours. Nat Rev Mater. 2016; 1 :16014.

(19). Lammers T, Kiessling F, Ashford M, Hennink WE, Crommelin D, Storm G. Cancer nanomedicine: is targeting our target. Nat Rev Mater. 2016; 1 :16069. [PubMed: 27668091]

(20). Lammers T. Macro-nanomedicine: Targeting the big picture. J Control Release. 2018; 294 :372. [PubMed: 30521831]

(21). Park K. The beginning of the end of the nanomedicine hype. J Control Release. 2019; 305 :221–222. [PubMed: 31170465]

(22). Lammers T, Kiessling F, Hennink WE, Storm G. Drug targeting to tumors: Principles, pitfalls and (pre-) clinical progress. J Control Release. 2012; 161 :175–187. [PubMed: 21945285]

(23). Arranja AG, Pathak V, Lammers T, Shi Y. Tumor-targeted nanomedicines for cancer theranostics. Pharmacol Res. 2017; 115 :87–95. [PubMed: 27865762]

(24). Hare JL, Lammers T, Ashford MB, Puri S, Storm G, Barry ST. Challenges and strategies in anti-cancer nanomedicine development: An industry perspective. Adv Drug Deliver Rev. 2017; 108 :25–38.

(25). Van der Meel R, Sulheim E, Shi Y, Kiessling F, Mulder WJM, Lammers T. Smart Cancer Nanomedicine. Nat Nanotechnol. 2019; 14 :1007–1017. [PubMed: 31695150]

(26). Hidalgo M, Amant F, Biankin AV, Budinská E, Byrne AT, Caldas C, Clarke RB, De Jong S, Jonkers j, Mælandsmo GM. Patient-derived xenograft models: an emerging platform for translational cancer research. Cancer Discov. 2014; 4 :998–1013. [PubMed: 25185190]

(27). Sharpless NE, DePinho RA. Model organisms: The mighty mouse: genetically engineered mouse models in cancer drug development. Nat Rev Drug Discov. 2006; 5 :741. [PubMed: 16915232]

(28). Gao H, Korn JM, Ferretti S, Monahan JE, Wang Y, Singh M, Zhang C, Schnell C, Yang G, Zhang Y. High-throughput screening using patient-derived tumor xenografts to predict clinical trial drug response. Nat Med. 2015; 21 :1318. [PubMed: 26479923]

(29). Shi Y, Van Der Meel R, Theek B, Oude Blenke E, Pieters EH, Fens MH, Ehling J, Schiffelers RM, Storm G, Van Nostrum CF, Lammers T, Hennink WE. Complete regression of xenograft tumors upon targeted delivery of paclitaxel via Π-Π stacking stabilized polymeric micelles. ACS Nano. 2015; 9 :3740–3752. [PubMed: 25831471]

(30). Shi Y, van Steenbergen MJ, Teunissenm EA, Novo L, Gradmann S, Baldus M, van Nostrum CF, Hennink WE. Π-Π stacking increases the stability and loading capacity of thermosensitive polymeric micelles for chemotherapeutic drugs. Biomacromolecules. 2013; 14 :1826–37. [PubMed: 23607866]

(31). Sheybanifard M, Beztsinna N, Bagheri M, Buhl EM, Bresseleers J, Varela-Moreira A, Shi Y, van Nostrum CF, van der Pluijm G, Storm G, Hennink WE. Systematic evaluation of design features enables efficient selection of Π electron-stabilized polymeric micelles. Int J Pharm. 2020; 7 :119409.

(32). Segelman J, Granath F, Holm T, Machado M, Mahteme H, Martling A. Incidence, prevalence and risk factors for peritoneal carcinomatosis from colorectal cancer. Brit J Surg. 2012; 99 :699–705. [PubMed: 22287157]

(33). Guo, j; Xu, A; Sun, X; Zhao, X; Xia, Y; Rao, H; Zhang, Y; Zhang, R; Chen, L; Zhang, T. Combined surgery and extensive intraoperative peritoneal lavage vs surgery alone for treatment of locally advanced gastric cancer: the SEIPLUS randomized clinical trial. JAMA Surg. 2019; 154 :610–616. [PubMed: 30916742]

(34). Marshall, J. Cell Migration. Humana Press; New Jersey. United States: 2011. 97–110.

(35). Pasqual EM, Bertozzi S, Londero AP, Brandolin D, Mariuzzi L, De Pellegrin A, Bacchetti S, Zoratti L, Petri R, Della Bianca C. Microscopic peritoneal carcinomatosis in gastric cancer: Prevalence, prognosis and predictive factors. Oncol Lett. 2018; 15 :710–716. [PubMed: 29399143]

(36). Vassos N, Piso P. Metastatic colorectal cancer to the peritoneum: Current treatment options. Curr Treat Options Oncol. 2018; 19 :49. [PubMed: 30173342]

(37). Kong JH, Lee J, Yi C-A, Park SH, Park JO, Park YS, Lim Y, Park KW, Kang WK. Lung metastases in metastatic gastric cancer: pattern of lung metastases and clinical outcome. Gastric Cancer. 2012; 15 :292–298. [PubMed: 22037917]

(38). Zampino MG, Maisonneuve P, Ravenda PS, Magni E, Casiraghi M, Solli P, Petrella F, Gasparri R, Galetta D, Borri A. Lung metastases from colorectal cancer: analysis of prognostic factors in a single institution study. Ann Thorac Surg. 2014; 98 :1238–1245. [PubMed: 25106681]

(39). Binnewies M, Roberts EW, Kersten K, Chan V, Fearon DF, Merad M, Coussens LM, Gabrilovich DL, Ostrand-Rosenberg S, Hedrick CC, CC. Understanding the tumor immune microenvironment (TIME) for effective therapy. Nat Med. 2018; 4 :541.

(40). Cullis J, Siolas D, Avanzi A, Barui S, Maitra A, Bar-Sagi D. Macropinocytosis of nab-paclitaxel drives macrophage activation in pancreatic cancer. Cancer Immunol Res. 2017; 5 :182–190. [PubMed: 28108630]

(41). Millrud CR, Mehmeti M, Leandersson K. Docetaxel promotes the generation of anti-tumorigenic human macrophages. Exp Cell Res. 2018; 362 :525–531. [PubMed: 29269075]

(42). Toka F, Dolega P, Mielcarska M, Bossowska M. Comparison of messenger RNA expression profile of antiviral innate immune response genes in peritoneal macrophages from BALB/c and C57BL/6 mice infected with ectromelia virus (INM3P. 413). J Immunol. 2015 :194. [PubMed: 26026056]

(43). Weiler S, Merz M, Kullak-Ublick GA. Drug-induced liver injury: the dawn of biomarkers? F1000 Med Rep. 2015 :7.

(44). Tentler JJ, Tan AC, Weekes CD, Jimeno A, Leong S, Pitts TM, Arcaroli JJ, Messersmith WA, Eckhardt SG. Patient-derived tumour xenografts as models for oncology drug development. Nat Rev Clin Oncol. 2012; 9 :338. [PubMed: 22508028]

(45). Siolas D, Hannon GJ. Patient-derived tumor xenografts: transforming clinical samples into mouse models. Cancer Res. 2013; 73 :5315–5319. [PubMed: 23733750]

(46). Miller MA, Zheng YR, Gadde S, Pfirschke C, Zope H, Engblom C, Kohler RH, Iwamoto Y, Yang KS, Askevold B, Kolishetti N. Tumour-associated macrophages act as a slow-release reservoir of nano-therapeutic Pt (IV) pro-drug. Nat Commun. 2015; 6 :1–3.

(47). Ruffell B, Coussens LM. Macrophages and therapeutic resistance in cancer. Cancer Cell. 2015; 27 :462–472. [PubMed: 25858805]

(48). Noy R, Pollard JW. Tumor-associated macrophages: from mechanisms to therapy. Immunity. 2014; 41 :49–61. [PubMed: 25035953]

(49). DeNardo DG, Ruffell B. Macrophages as regulators of tumour immunity and immunotherapy. Nat Rev Immunol. 2019; 19 :369–382. [PubMed: 30718830]

(50). Peranzoni E, Lemoine J, Vimeux L, Feuillet V, Barrin S, Kantari-Mimoun C, Bercovici N, Guérin M, Biton J, Ouakrim H. Macrophages impede CD8 T cells from reaching tumor cells and limit the efficacy of anti-PD-1 treatment. Proc Natl Acad Sci. 2018; 115 E4041-E4050 [PubMed: 29632196]

(51). Rodell CCB, Arlauckas SP, Cuccarese MF, Garris CS, Li R, Ahmed MS, Kohler RH, Pittet MJ, Weissleder R. TLR7/8-agonist-loaded nanoparticles promote the polarization of tumour-associated macrophages to enhance cancer immunotherapy. Nat Biomed Eng. 2018; 2 :578. [PubMed: 31015631]

(52). Chen Q, Wang C, Zhang X, Chen G, Hu Q, Li H, Wang J, Wen D, Zhang Y, Lu Y. In situ sprayed bioresponsive immunotherapeutic gel for post-surgical cancer treatment. Nat Nanotechnol. 2019; 14 :89–97. [PubMed: 30531990]

(53). Zanganeh S, Hutter G, Spitler R, Lenkov O, Mahmoudi M, Shaw A, Pajarinen JS, Nejadnik H, Goodman S, Moseley M. Iron oxide nanoparticles inhibit tumour growth by inducing pro-inflammatory macrophage polarization in tumour tissues. Nat Nanotechnol. 2016; 11 :986. [PubMed: 27668795]

(54). Anselmo AC, Mitragotri S. Nanoparticles in the clinic: An update. Bioeng Transl Med. 2019; 4 e10143 [PubMed: 31572799]

(55). Hua S, De Matos MB, Metselaar JM, Storm G. Current trends and challenges in the clinical translation of nanoparticulate nanomedicines: pathways for translational development and commercialization. Front Pharmacol. 2018 :9. [PubMed: 29422861]

(56). Ioannidis JP, Kim BY, Trounson A. How to design preclinical studies in nanomedicine and cell therapy to maximize the prospects of clinical translation. Nat Biomed Eng. 2018; 2 :797. [PubMed: 30931172]

(57). Anchordoquy TJ, Barenholz Y, Boraschi D, Chorny M, Decuzzi P, Dobrovolskaia MA, Farhangrazi ZS, Farrell D, Gabizon A, Ghandehari H. Mechanisms and barriers in cancer nanomedicine: addressing challenges, looking for solutions. ACS Nano. 2017; 11 :12–18. [PubMed: 28068099]

(58). Golombek SK, May J-N, Theek B, Appold L, Drude N, Kiessling F, Lammers T. Tumor targeting via EPR: Strategies to enhance patient responses. Adv Drug Deliv Rev. 2018; 130 :17–38. [PubMed: 30009886]

(59). Lammers T, Rizzo LY, Storm G, Kiessling F. Personalized nanomedicine. Clin Cancer Res. 2012; 18 :4889–4894. [PubMed: 22829203]

(60). Von Minckwitz G, Schmitt WD, Loibl S, Müller BM, Blohmer JU, Sinn BV, Eidtmann H, Eiermann W, Gerber B, Tesch H, Hilfrich J. Ki67 measured after neoadjuvant chemotherapy for primary breast cancer. Clin Cancer Res. 2013; 19 :4521–31. [PubMed: 23812670]

(61). Zhang X, Chen F, Huang Z. Apoptosis induced by acrylamide is suppressed in a 21.5% fat diet through caspase-3-independent pathway in mice testis. Toxicol Mech Method. 2009; 19 :219–24.

Europe PMC Funders Author Manuscripts

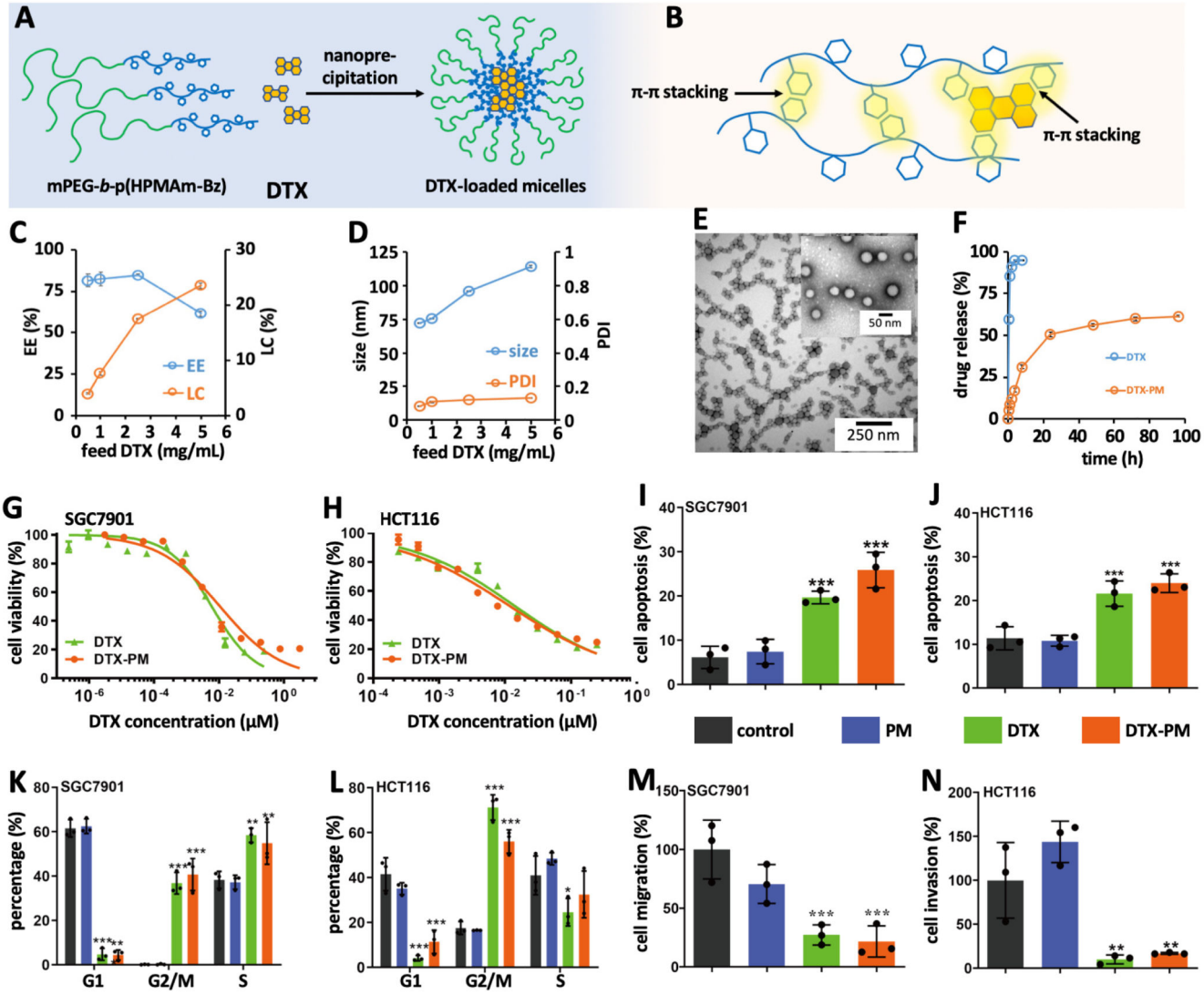

Figure 1. Preparation docetaxel-loaded Π electron-stabilized polymeric micelles (DTX-PM).

A : DTX was formulated in mPEG-b-p(HPMAm-Bz)-based PM via nanoprecipitation. B: The aromatic groups of the polymer and DTX allow for high and stable drug loading, via Π-Π stacking interactions. C: Encapsulation efficiency (EE) and loading capacity (LC) of DTX in PM. D: Size and polydispersity index of DTX-PM. E: TEM images of DTX-PM with 1 mg/mL of DTX. F: Release kinetics of free DTX and DTX-PM under sink conditions via a dialysis membrane against a medium containing 4.5% bovine serum albumin. G and H: In vitro cytotoxicity of free DTX and DTX-PM in SGC7901 human gastric cancer and HCT116 human colon carcinoma cells, as assessed by the CCK8 assay. The concentrations of IC50 of the free drug or DTX-PM in each cell line were used in following in vitro studies. I and J: Apoptosis induction upon treatment with DTX-PM, free DTX at the IC50 of each cell line and empty PM, as assessed by flow cytometry. K and L: Flow cytometry-based cell cycle analysis, showing prominent G2/M cell cycle arrest upon treatment with both DTX-PM and free DTX. M and N: Assessments of the anti-migration and anti-invasion

properties of DTX-PM in SGC7901 cells using the transwell assay. *, ** and *** indicate P<0.05, 0.01, and 0.001, respectively (versus PBS and empty PM).

Europe PMC Funders Author Manuscripts

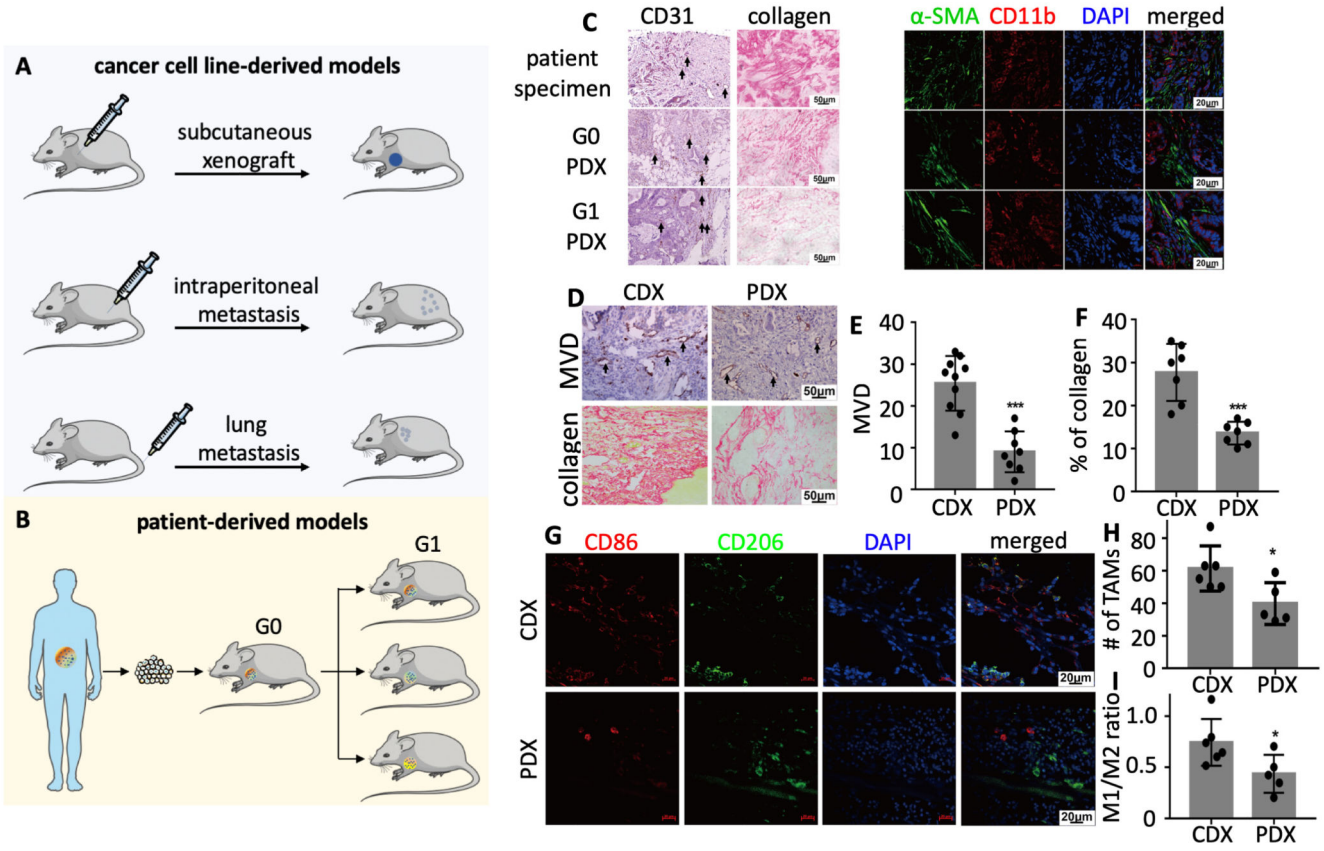

Figure 2. Cell line- and patient-derived mouse models for advanced-stage GI cancer.

A: Cell line-derived xenografts (CDX) were generated using SGC7901 human gastric cancer cells, and included subcutaneous tumors, intraperitoneal metastasis and lung metastasis in mice. B: Patient-derived xenografts (PDX) were generated by implanting tumor tissue derived from an advanced-stage colorectal cancer patient in mice, growing a generation 0 tumor, and by then transplanting G0 tumor tissue to a larger number of mice with G1 tumors. C: Histopathological and immunofluorescence analysis of the PDX models, showing that - apart from collagen content - there were no obvious differences between the original patient tumor and the G0 and G1 PDX tumors. CD31: Blood vessels. Ki67: Proliferating cells. α-SMA: Fibroblasts. CD11b: Macrophages of both mouse and human origin. DAPI: Nuclei. D-I: Histopathological and immunofluorescence analysis of CDX and PDX tumors. CDX tumors presented with higher microvessel density (MVD), more collagen and more macrophages. CD86: M2-like macrophages. CD206: M2-like macrophages. *: $P < 0.05$, **: $P < 0.01$, and ***: $P < 0.001$.

Europe PMC Funders Author Manuscripts

Europe PMC Funders Author Manuscripts

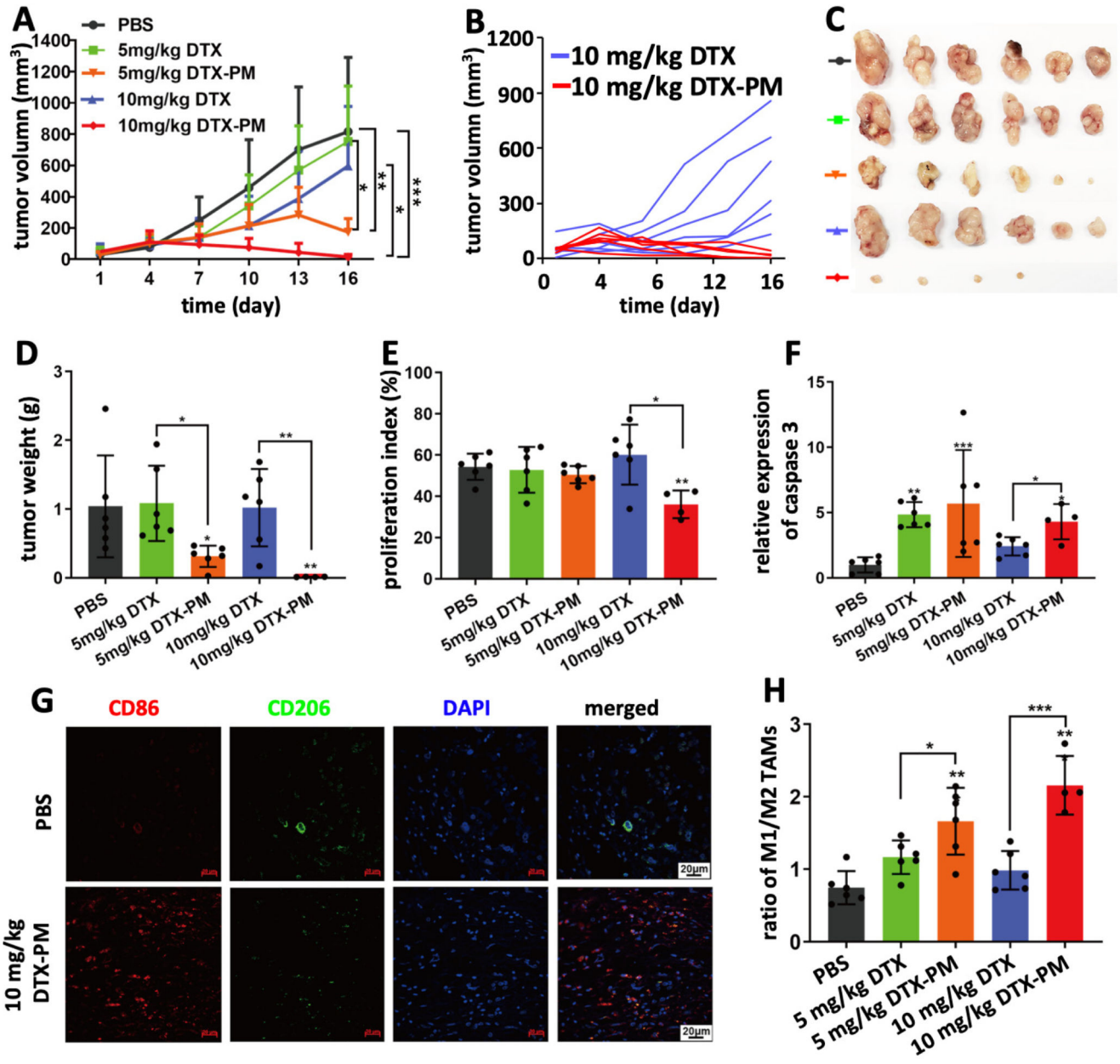

Figure 3. Inhibition of SGC7901 cell line-derived subcutaneous xenografts by DTX-PM.

A: Tumor growth curves of mice treated 5 times with PBS, DTX and DTX-PM at 5 and 10 mg/kg, showing that DTX-PM were more effective than free DTX. B-D: DTX-PM dosed at 10 mg/kg was able to completely eradicate tumors in almost all mice. E and F: Proliferation and apoptosis assessed by immunohistochemical staining Ki67 and cleaved caspase 3. G: The polarization of tumor-associated macrophages (TAM) was studied by immunofluorescence staining. H: Calculation of the ratio between M1-like macrophages (CD86 staining; red) and M2-like TAM (CD206 staining; green) showed that significantly more M1-like TAM were present upon treatment with DTX-PM. Values are mean ± SD. *: $P < 0.05$, **: $P < 0.01$, and ***: $P < 0.001$.

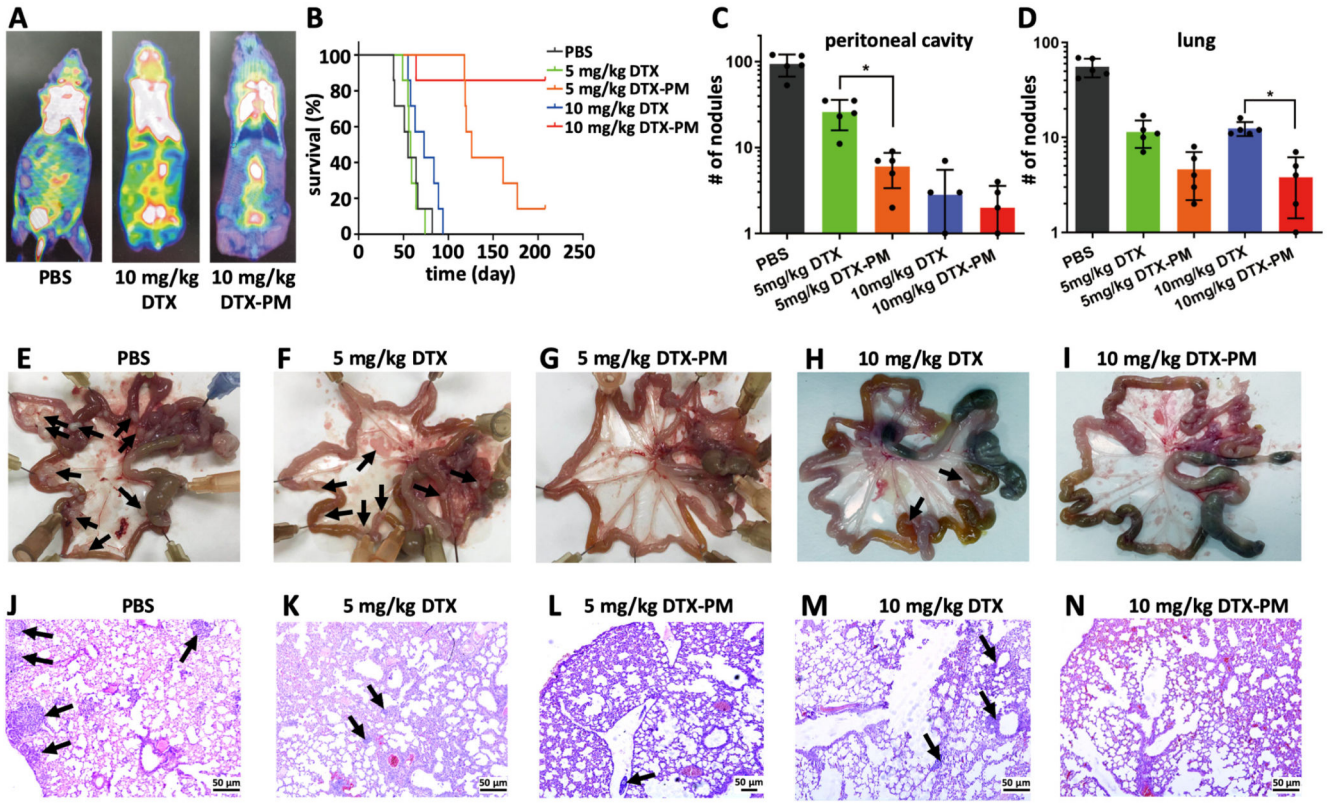

Figure 4. PM improve DTX efficacy in metastatic CDX models of GI cancer.

A: 18F-FDG-based PET-CT imaging of peritoneal metastasis upon treatment with PBS, 10 mg/kg DTX and 10 mg/kg DTX-PM at day 16. B: Survival of mice with peritoneal GI cancer metastasis upon five administrations of PBS, DTX and DTX-PM at 5 and 10 mg/kg. C-N: Assessment of metastatic nodules in the peritoneal cavity (C) and in the lungs (D), based on macroscopic quantifications in the intestines of mice (E-I) and on microscopic analyses of the lungs of mice (J-N). Metastatic nodules are indicated by black arrows. Values represent mean ± SD. *: $P < 0.05$, **: $P < 0.01$, and ***: $P < 0.001$.

Europe PMC Funders Author Manuscripts

Europe PMC Funders Author Manuscripts

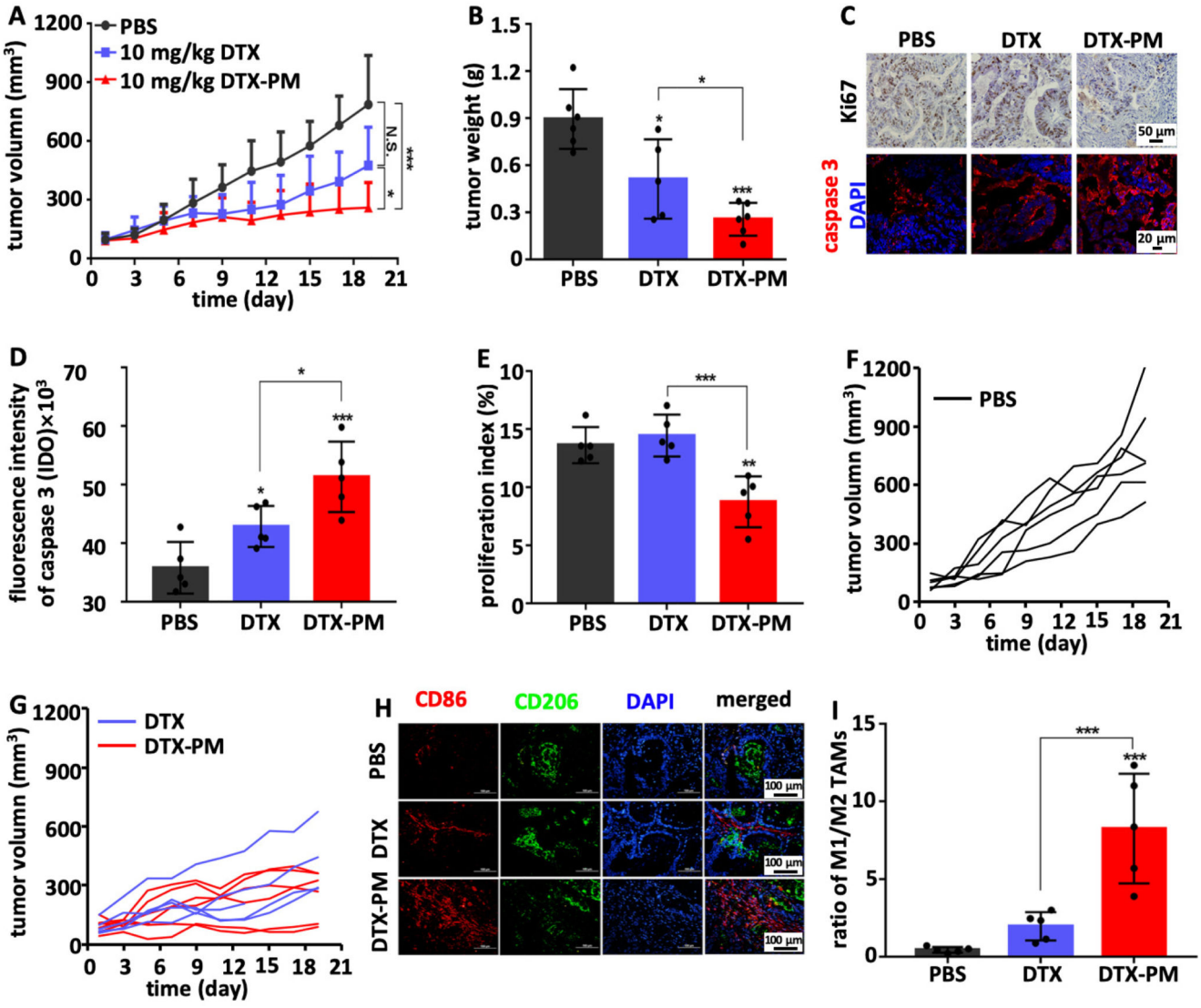

Figure 5. DTX-PM improve DTX efficacy in a PDX model of GI cancer.

A: Tumor growth inhibition upon treatment with PBS, and with 10 mg/kg of free DTX and DTX-PM. B: Tumor weights at the end of the experiment, showing significantly more efficient tumor inhibition for DTX-PM than for free DTX. C-E: Immunofluorescence analysis of cellular proliferation (Ki67) and apoptosis induction (cleaved caspase 3), confirming that DTX-PM was more effective than free DTX. F and G: Individual PDX tumor growth curves in the mice treated with DTX and DTX-PM as compared to PBS controls, exemplifying the superior efficacy of DTX-PM. H and I: PDX tumors were analyzed by means of immunofluorescence microscopy, showing a substantially increased ratio of M1-like to M2-like TAM upon DTX-PM treatment.